Carrier heating in intrinsic graphene by a strong dc electric field

O. G. Balev
Departamento de Fisica, Universidade Federal do Amazonas, Manaus 69077-000, Brazil

F. T. Vasko*
Institute of Semiconductor Physics, NAS of Ukraine, Pr. Nauki 41, Kiev 03028, Ukraine

V. Ryzhii
University of Aizu, Ikki-machi, Aizu-Wakamatsu 965-8580, Japan
and Japan Science and Technology Agency, CREST, Tokyo 107-0075, Japan

(Received 17 January 2009; revised manuscript received 1 April 2009; published 24 April 2009)

We consider the heating of carriers in an intrinsic graphene in a strong dc electric field. The intraband energy relaxation due to acoustic phonon scattering and the interband generation-recombination transitions due to thermal radiation are taken into account. The distributions of nonequilibrium carriers are obtained for the cases when the carrier-carrier scattering is unessential and when the intercarrier Coulomb scattering effectively establishes the quasiequilibrium distribution with the temperature and the density of carriers determined by the balance equations. Due to an interplay between weak energy relaxation and generation-recombination processes, the nonlinear response is characterized by a very low threshold electric field. The nonlinear current-voltage characteristics as well as the field-dependent carrier concentration are calculated for the case of the momentum relaxation associated with the elastic scattering. The obtained current-voltage characteristics exhibit a low threshold of nonlinearity and an appearance of the second ohmic region, for strong fields.

DOI: 10.1103/PhysRevB.79.165432 PACS number(s): 73.50.Fq, 81.05.Uw

I. INTRODUCTION

Active studies of graphene in recent years are stimulated by unusual physical properties of this gapless and massless semiconductor (see discussion and references in the review[1]) as well as the prospects its applications in electronics (see, for instance, Refs. 1 and 2, and the references therein). For different device applications of graphene, the in-depth understanding of its optical and electrical properties, particularly, far from equilibrium, is indispensable. Both experimental and theoretical studies of the nonequilibrium carriers in graphene under interband photoexcitation have been already performed (see Ref. 3 and Refs. 4 and 5, respectively, and references therein). Experimental investigations of the carrier heating in graphene by a dc electric field were carried out in relation with demonstrations of a graphene field-effect transistor.[6] Essential heating apparently had occurred in the experiments on current-induced cleaning of graphene.[7] The theoretical treatments of the rate of energy relaxation of nonequilibrium carries were performed both analytically[8] and numerically.[9] The kinetic equation for carriers in graphene in a strong electric field was recently derived and discussed.[10] Nevertheless, the basic problem of the carrier heating in graphene by a dc electric field has not been considered in a systematic way and the graphene current-voltage characteristics were not analyzed yet.

In this paper, we study a heating of carriers in an intrinsic graphene under the effect of a dc electric field. To describe these phenomena, we take into account both an increase in the energy of carries in the electric field, **E**, and the following relaxation processes: (1) the relaxation of the carrier momentum due to elastic scattering on the structural disorder (this is the most fast process ensuring weak anisotropy of the carrier distribution function[11]), (2) the intraband quasielastic energy relaxation on acoustic phonons, (3) the generation-recombination processes due to interband transitions induced by thermal radiation, and (4) the intercarrier scattering due to the Coulomb interaction. In the present study, we consider the carrier heating within the following two limiting regimes: (i) the regime when the Coulomb interaction is unessential, so that it is possible to neglect the intercarrier scattering, and (ii) the Coulomb-controlled regime. In the latter case, the Coulomb scattering provides the quasiequilibrium distribution of carries, with the distribution characteristics described by the equations of the concentration balance and the energy balance. We find the distribution functions of carries for these regimes and investigate their dependences on the applied electric field and on the temperature of thermostat formed by phonons and thermal radiation. In addition, we analyze the concentration of the nonequilibrium carriers and the current-voltage characteristics.

The character of the obtained nonlinear response is determined by the following features of the model under consideration. First, the carrier velocity, $v_W\mathbf{p}/p$, does not increase with the energy, where $v_W=10^8$ cm/s is the characteristic velocity of charged neutrinolike particles, and $\mathbf{p}$ is the two-dimensional (2D) momentum. Second, the interband transitions are effectively excited by thermal radiation (the matrix element of transition is $\propto v_W$) and they not only affect the carrier concentration but also substantially contribute to the carrier energy relaxation. As a result, the nonequilibrium distributions are formed due to the interplay between a weak-energy relaxation and generation-recombination processes (i.e., due to the interplay between the interactions of carriers with phonon and photon thermostats). Third, although the interaction of carriers with small momentum p with phonons is weak, the rate of energy relaxation sharply rises with the momentum increase. Therefore, for scattering on short-range

defects, when the relaxation of momentum grows with the energy, it is realized a sublinear current-voltage characteristic with essential nonlinearity for weak fields. If the momentum relaxation becomes ineffective for high-energy carriers (because of a finite-range disorder) a superlinear increase in current takes place. In the region of strong fields a linear current-voltage characteristic is realized (the second ohmic region) where the effective conductivity is smaller than the conductivity of equilibrium carriers for low temperatures, T.

The paper is organized in the following way. The basic equations governing the processes of the heating of carriers in an intrinsic graphene under a dc electric field are presented in Sec. II. In Sec. III, we consider the symmetric parts of the distribution functions of nonequilibrium carriers for cases (i) and (ii) and we calculate the carrier concentration as function of field. The current-voltage characteristics are analyzed in Sec. IV. The concluding remarks and discussion of the assumptions used are given in Sec. V. In the Appendix, the general equation for the density matrix is reduced to the quasiclassic kinetic equation for the carrier distribution function in a dc electric field used in the paper.

II. BASIC EQUATIONS

Nonequilibrium carriers, electrons, and holes in the intrinsic graphene are described by coinciding distribution functions $f_{e,\mathbf{p}}=f_{h\mathbf{p}}\equiv f_{\mathbf{p}}$ as their energy spectra are symmetric and the scattering mechanisms are identical (see the Appendix). Therefore, instead of system of the kinetic equations for $f_{e\mathbf{p}}$ and $f_{h\mathbf{p}}$, one can consider the following kinetic equation:

$$e\mathbf{E}\cdot\frac{\partial f_{\mathbf{p}}}{\partial \mathbf{p}}=\sum_j J_j\{f|\mathbf{p}\}. \tag{1}$$

Here, $\mathbf{E}$ is the electric field and $J_j\{f|\mathbf{p}\}$ is the collision integral for the jth scattering mechanism, with the indices $j=D$, LA, R, and C corresponding to the static disorder (D), the acoustic phonon scattering (LA), the radiative-induced interband transitions (R), and the carrier-carrier scattering (C), respectively. The collision integral for the elastic scattering was considered previously[11,12] (see also the references therein), $J_{LA}\{f|\mathbf{p}\}$ and $J_R\{f|\mathbf{p}\}$ were evaluated in Ref. 5, and the Coulomb scattering integral was considered in Ref. 13. For the distribution function obeying Eq. (1), the equation governing the concentration balance can be presented as

$$\frac{4}{L^2}\sum_{\mathbf{p}} J_R\{f|\mathbf{p}\}=0. \tag{2}$$

Equation (2) accounts for the fact that the interband transitions are forbidden not only for elastic scattering but also for Coulomb scattering, due to symmetry of the energy spectrum,[14] and for the phonon scattering, due to the condition $s\ll v_W$. Here s is the velocity of sound. The factor 4 in Eq. (2) takes into account the spin and valley degeneracies, and L^2 is the normalization area.

Taking into account that electrons and holes equally contribute to the current density, $\mathbf{I}$, one obtains

$$\mathbf{I}=\frac{8ev_W}{L^2}\sum_{\mathbf{p}}\frac{\mathbf{p}}{p}\Delta f_{\mathbf{p}}. \tag{3}$$

Here, the asymmetric part of distribution function, $\Delta f_{\mathbf{p}}$, is separated from the symmetric one, f_p, by using the relation $f_{\mathbf{p}}=f_p+\Delta f_{\mathbf{p}}$. At $|e\mathbf{E}|\tau_p^{(m)}\ll p$, where $\tau_p^{(m)}$ is the momentum relaxation time, the asymmetric part is relatively small:[15] $|\Delta f_{\mathbf{p}}|\ll f_p$. As follows from Eq. (1), $\Delta f_{\mathbf{p}}$ is given by

$$\Delta f_{\mathbf{p}}=\frac{(e\mathbf{E}\cdot\mathbf{p})}{p}\tau_p^{(m)}\left(-\frac{df_p}{dp}\right). \tag{4}$$

In the case of a random potential $U_{\mathbf{x}}$ characterized by the correlation function $\langle U_{\mathbf{x}}U_{\mathbf{x}'}\rangle\equiv\overline{U_d}^2\exp\{-[(\mathbf{x}-\mathbf{x}')/l_c]^2\}$ with the averaged energy $\overline{U_d}$ and the correlation length l_c, one obtains[11]

$$\frac{1}{\tau_p^{(m)}}=\frac{v_d p}{\hbar}\Psi\left(\frac{pl_c}{\hbar}\right),\quad \Psi(z)=\frac{e^{-z^2}}{z^2}I_1(z^2), \tag{5}$$

where the characteristic velocity v_d is introduced as $v_d=\pi\overline{U}_d^2 l_c^2/4\hbar^2 v_W$. The form factor $\Psi(z)$, which is expressed via the modified Bessel function $I_1(x)$, decreases with $pl_c/\hbar$. The conductivity of graphene, σ, is determined by the standard formula $\mathbf{I}=\sigma\mathbf{E}$. Using Eqs. (3)–(5) and performing the averaging over angle, the expression for the conductivity can be presented as

$$\sigma=\frac{e^2}{\pi\hbar}\frac{2v_W}{v_d}\int_0^\infty\frac{dp}{\Psi(pl_c/\hbar)}\left(-\frac{df_p}{dp}\right). \tag{6}$$

Next, averaging Eq. (1) over the angle (below we symbolize such an averaging by a line over the expression) and neglecting the weak contribution of $\Delta f_{\mathbf{p}}$ to the right-hand side of Eq. (1), we reduce the kinetic equation for the symmetric part f_p of the distribution function to the following form:

$$\overline{e\mathbf{E}\cdot\frac{\partial\Delta f_{\mathbf{p}}}{\partial\mathbf{p}}}=\sum_j J_j\{f|p\}. \tag{7}$$

Here $J_j\{f|p\}=\overline{J_j\{t|\mathbf{p}\}}$ and summation is performed over $j=LA$, R, and C because the elastic scattering does not affect the symmetric distribution due to the energy conservation. The left-hand side of Eq. (7), which describes the effect of the electric field, can be presented as follows:[16]

$$\overline{e\mathbf{E}\cdot\frac{\partial\Delta f_{\mathbf{p}}}{\partial\mathbf{p}}}=\frac{(eE)^2}{2p}\frac{d}{dp}p\tau_p^{(m)}\left(-\frac{df_p}{dp}\right). \tag{8}$$

As a result, using the Fokker-Planck form of $J_{LA}\{f|p\}$ and $J_R\{f|p\}$ obtained in Ref. 5, we arrive at the following kinetic equation:

$$\frac{\nu_p^{(qe)}}{p^2}\frac{d}{dp}\left\{\left[p^4+\frac{p_E^4}{2\Psi(pl_c/\hbar)}\right]\frac{df_p}{dp}+\frac{p^4}{p_T}f_p(1-f_p)\right\}+\nu_p^{(R)}[N_{2p/p_T}(1-2f_p)-f_p^2]+J_C\{f|p\}=0, \tag{9}$$

where $N_x=(e^x-1)^{-1}$ is the Planck distribution function and $p_T=T/v_W$, with the equilibrium temperature T. The rate of quasielastic energy relaxation $\nu_p^{(qe)}$ and of the rate of radia-

tive transitions $\nu_p^{(R)}$ can be presented, respectively, in the form[5]

$$\nu_p^{(qe)} = \left(\frac{s}{v_W}\right)^2 \frac{v_{ac}p}{\hbar}, \quad v_{ac} = \frac{D^2 T}{4\hbar^2 \rho_s v_W s^2},$$

$$\nu_p^{(R)} = \frac{v_r p}{\hbar}, \quad v_r = \frac{e^2\sqrt{\epsilon}}{\hbar c}\left(\frac{v_w}{c}\right)^2 \frac{8v_W}{3}. \tag{10}$$

Here we have introduced the characteristic velocities v_{ac} and v_r expressed via the deformation potential D, the sheet density of graphene ρ_s, and the dielectric permittivity ϵ. The characteristic momentum p_E in Eq. (9) is defined as

$$p_E^4 = \left(\frac{v_W}{s}\right)^2 \frac{(eE\hbar)^2}{v_{ac}v_d} \tag{11}$$

so that $p_E \propto \sqrt{E}$. The Coulomb scattering integral $J_C\{f|p\}$ can be neglected in Eq. (9) for case (i). In this case, the nonequilibrium distribution function f_p is governed by a nonlinear differential equation of the second order.

In case (ii), the Coulomb scattering term in Eq. (9) is dominant so that it provides the quasiequilibrium distribution described by the following function:

$$\tilde{f}_p = \{\exp[(v_W p - \mu)/T_c] + 1\}^{-1}, \tag{12}$$

with the effective temperature of carriers T_c and the quasichemical potential μ. To determine T_c and μ, we can use the concentration balance Eq. (2) and the energy balance equation. The latter we derive by summing Eq. (7) over $\mathbf{p}$ with the energy weight $v_W p$ as follows:

$$\frac{1}{2}\sigma E^2 + \frac{4v_W}{L^2}\sum_{\mathbf{p}} p[J_{LA}(f|p) + J_R(f|p)] = 0. \tag{13}$$

The field term in Eq. (13) is expressed through conductivity (6) using the integration by parts (the factor 1/2 is quite understood as the total Joule heat σE^2 is shared equally between electrons and holes). Therefore, the parameters characterizing $\tilde{f}_p$, i.e., T_c and μ, are governed by two transcendent Eqs. (2) and (13). After that, the nonlinear conductivity can be calculated substituting $\tilde{f}_p$ into Eq. (6).

III. NONEQUILIBRIUM DISTRIBUTIONS

Below we consider the nonequilibrium distribution functions obtained from Eq. (9) with the Coulomb contribution omitted [case (i)] or from the balance Eqs. (2) and (13) [case (ii)]. Also we present the field and temperature dependences of the nonequilibrium carrier concentration.

A. Weak intercarrier scattering

We start with consideration of case (i), when the carrier-carrier scattering is ineffective. Omitting J_C in Eq. (9) and introducing the dimensionless momentum $x=p/p_T$ and the parameter $\eta=p_T l_c/\hbar$, we obtain the nonlinear differential equation as follows:

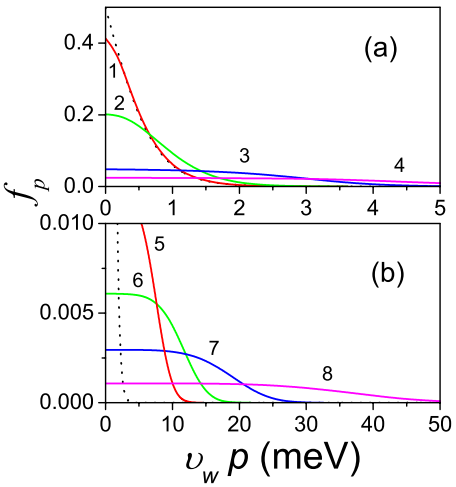

FIG. 1. (Color online) Determined from Eq. (14) distribution functions, at $T=4.2$ K and $l_c=10$ nm: (a) for weak electric fields (1) $E=0.1$ mV/cm, (2) 1 mV/cm, (3) 10 mV/cm, and (4) 30 mV/cm; (b) for strong electric fields $E=0.1$ V/cm (5), 0.3 V/cm (6), 1 V/cm (7), and 5 V/cm (8). Dotted curves correspond to the equilibrium distribution.

$$\frac{d}{dx}\left\{\left[x^4 + \frac{(p_E/p_T)^4}{2\Psi(x\eta)}\right]\frac{df_x}{dx} + x^4 f_x(1-f_x)\right\} + \Gamma x^2\left(\frac{1-2f_x}{e^{2x}-1} - f_x^2\right) = 0. \tag{14}$$

Here, the dimensionless parameter $\Gamma=(v_W/s)^2 v_r/v_{ac}$ determines the relative contribution of the thermal radiation and energy relaxation. As the boundary conditions for Eq. (14) we use the following one: $x^4(df_x/dx+f_x)_{x\to\infty}=0$, so that f_x must decrease at $x\to\infty$ sufficiently fast[15] and also the density balance Eq. (2). Integrating Eq. (14) over x from 0 to ∞ in order to write the balance equation, we obtain an additional term proportional to $(p_E/p_T)^4(df_x/dx)_{x=0}$, which must be equal to zero. As a result, we obtain $(df_x/dx)_{x\to 0}=0$ and this requirement can be used as the second boundary condition for Eq. (14) [instead of Eq. (2)].

The numerical solution of Eq. (14) was performed applying the finite difference method and the iterations over nonlinear contributions (see Ref. 17). The distribution functions calculated for different temperatures, electric fields, and l_c are presented in Figs. 1 and 2. In the range of low temperatures, the distribution function exhibits two different types of behavior with increasing electric field: in weak electric fields, $(p_E/p_T)^4/(4\Gamma) \ll 1$, and in strong electric fields, $(p_E/p_T)^4/(4\Gamma) \gg 1$.

As it is seen from Figs. 1(a) and 2, in weak electric fields there is an essential suppression of the distribution function in the range of small $p<p_T$ (as slow carriers are heated very effectively), while in the range of large $p>p_T$, the distribution function remains almost equilibrium one. Further, Figs. 1 and 2 show also that as the electric field becomes strong, the carriers are spread over a wide range of energies such that, e.g., at $T=4.2$ K for $E>5$ V/cm, the tail of the distribution will reach the energies for which the spontaneous emission of the optical phonons begins (~90 meV). It can be seen as well that with an increase in T the transition

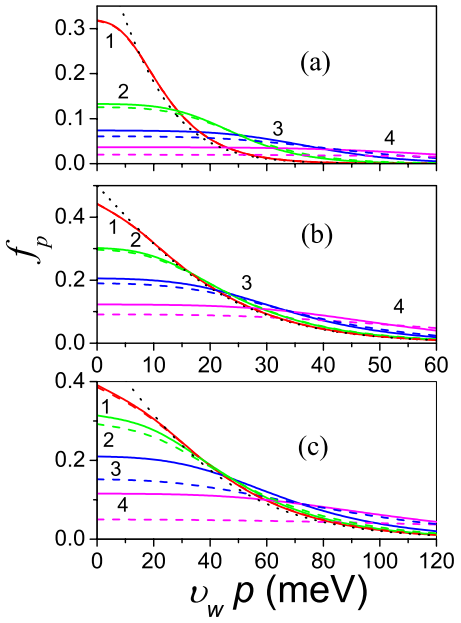

FIG. 2. (Color online) The same as in Fig. 1 calculated: (a) for (1) $T=77$ K and $E=0.14$ V/cm, (2) 1.4 V/cm, (3) 4.4 V/cm, and (4) 14 V/cm; (b) for (1) $T=150$ K and $E=74$ mV/cm, (2) 0.74 V/cm, (3) 2.35 V/cm, and (4) 7.4 V/cm; (c) for (1) $T=300$ K and $E=1$ V/cm, (2) 3 V/cm, (3) 10 V/cm, and (4) 30 V/cm. The solid and the dashed curves correspond to $l_c=10$ nm and 20 nm, respectively. Dotted curves correspond to equilibrium distributions.

between the weak-field and strong-field regimes occurs at a higher electric field $E \propto T^2$. Figures 2(a)–2(c) show the plots of the distribution functions calculated for $l_c=10$ nm and 20 nm and different E and T. It is seen that the effect of a finite l_c reinforces with increasing E so that the influence of the electric field on the distribution function becomes more pronounced at higher l_c. However, at weak E the difference between the solid and dashed curves is practically invisible. Notice, from the solid and, especially, the dashed curves 4 in Fig. 2(c) it follows that in the case in question the interaction with optical phonons can be important.

B. Coulomb-controlled distribution

Further, we examine case (ii), when quasiequilibrium distribution given by Eq. (12) is determined from the balance equations, Eqs. (2) and (13). Introducing the dimensionless momentum, $y=v_W p/T_c$, so that $\tilde{f}_y=[\exp(y-\mu/T_c)+1]^{-1}$, we rewrite the concentration balance Eq. (2) in the form

$$\int_0^\infty dy y^2 \left(\frac{1-2\tilde{f}_y}{e^{2yT_c/T}-1} - \tilde{f}_y^2 \right) = 0. \tag{15}$$

Equation (15) yields the relation between μ/T and dimensionless temperature T_c/T (this relation is not dependent explicitly on the electric field). Simultaneously, the energy balance Eq. (13) can be presented as

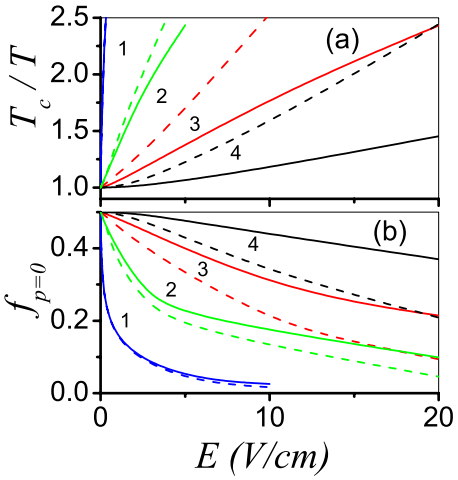

FIG. 3. (Color online) Determined from the balance Eqs. (15) and (16) (a) dimensionless effective temperature T_c/T and (b) maximal distribution $\tilde{f}_{p=0}$ versus electric field for (1) $T=20$ K, (2) 77 K, (3) 150 K, and (4) 300 K. Solid and dashed curves are correspondent to $l_c=10$ nm and 20 nm, respectively.

$$Q_E - \frac{T_c - T}{T} \int_0^\infty dy y^4 e^{y-\mu/T_c} \tilde{f}_y^2 + \Gamma \int_0^\infty dy y^3 \left(\frac{1-2\tilde{f}_y}{e^{2yT_c/T}-1} - \tilde{f}_y^2 \right) = 0, \tag{16}$$

where field contribution Q_E is transformed using Eq. (6),

$$Q_E = \left(\frac{p_E}{T_c/v_W} \right)^4 \left[\tilde{f}_{y=0} + \frac{\eta_c}{2} \int_0^\infty dy \tilde{f}_y \Phi(\eta_c y) \right]. \tag{17}$$

Here $\eta_c = T_c l_c/\hbar v_W$ and $\Phi(z) = -\Psi'(z)/\Psi(z)^2$ with $\Psi(0)=1/2$.

In Figs. 3(a) and 3(b), the dimensionless effective temperature T_c/T and the maximal value of the distribution function $\tilde{f}_{p=0}=[\exp(-\mu/T_c)+1]^{-1}$, which are calculated from Eqs. (15) and (16), are shown as functions of E for different T. As seen from Fig. 3(a), the dimensionless temperature T_c/T rises faster with increasing electric field E for larger l_c; in addition, an increase in T_c/T becomes steepened at smaller T. Figure 3(b) shows that the characteristic value, $f_{p=0}$, of distribution function decreases faster with increasing E at smaller T.

C. Hot carrier concentration

Using the solutions of Eq. (14) or Eqs. (15)–(17), below we calculate the carrier concentration

$$n = \frac{2}{\pi\hbar^2} \int_0^\infty dp p f_p, \tag{18}$$

where f_p in the right-hand side of Eq. (18) should be replaced by $\tilde{f}_p$ in case (ii). As a result, the electric field dependence of n is determined by a competition of an increase in the effective temperature T_c and a decrease in the maximal distribution $\tilde{f}_{p=0}$ [see Figs. 3(a) and 3(b)]. Hence, the carrier

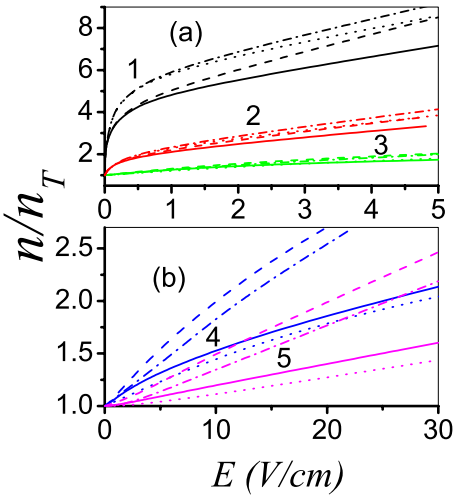

FIG. 4. (Color online) Normalized carrier concentration, n/n_T, versus electric field: (a) at (1) $T=4.2$ K, (2) 20 K, (3) 77 K, and (b) at (4) $T=150$ K, (5) 300 K. The solid and the dashed curves are calculated from Eqs. (14) and (18) for $l_c=10$ nm and 20 nm, respectively. The dotted and the dot-dashed curves are calculated from Eqs. (15)–(18) for $l_c=10$ nm and 20 nm, respectively.

concentration increases slowly when the electric field increases.

Figure 4 shows the plot of the dimensionless carrier concentration n/n_T as a function of E. Here the equilibrium concentration readily follows from Eq. (18) as $n_T=\pi(T/\hbar v_W)^2/6$ [notice, at $T=4.2$, 20, 77, 150, and 300 K one obtains $n_T=1.6\times10^7$ cm^{-2}, 3.6×10^8 cm^{-2}, 5.4×10^9 cm^{-2}, 2.0×10^{10} cm^{-2}, and 8.1×10^{10} cm^{-2}, respectively]. From Fig. 4 one can see the following: (a) at low temperatures (and not too large E), the relative increase in the density $(n-n_T)/n_T$ is approximately proportional to $E^{1/2}$ because due to a small characteristic momentum $\bar{p}$, the effect of a finite l_c is negligible; (b) at higher temperatures (or very large E), $(n-n_T)/n_T$ is a linear function of E, i.e., $(n-n_T)/n_T\approx A+BE$, because due to large $\bar{p}$, the effect of a finite l_c becomes essential. Notice, that the carrier-concentration increase becomes faster for larger l_c.

IV. CURRENT-VOLTAGE CHARACTERISTICS

Using the nonequilibrium distribution functions obtained in Sec. III, we calculate here the nonlinear conductivity given by Eq. (6) and analyze the modifications of the current-voltage characteristics due to variations in the temperature and l_c. Performing the integration in Eq. (6) by parts, we arrive at

$$\sigma=\sigma_0\left[2f_{p=0}+\frac{l_c}{\hbar}\int_0^\infty dpf_p\Phi(pl_c/\hbar)\right], \tag{19}$$

where $\sigma_0=(2v_W/v_d)e^2/\pi\hbar$ is the characteristic conductivity. For the case of short-range scattering ($\bar{p}l_c/\hbar\ll1$, where $\bar{p}$ is the characteristic momentum of hot carriers), the conductivity can be expressed via the distribution function of low-energy carriers as follows: $\sigma\simeq2\sigma_0f_{p=0}$. Since $f_{p=0}=1/2$, in the limit $E\to0$ one obtains $\sigma=\sigma_0$ in the case of short-range scattering and in the absence of heating. In Fig. 5 we plot σ/σ_0 versus electric field E for $l_c=10$ nm. Notice, in Figs. 5(a)–5(c), except the inset in Fig. 5(a), the same electric field range is considered; it is different from that used in Figs. 5(d) and 5(e). It is seen that both approaches yield similar dependences even for very strong fields for given T and l_c. The dependences σ/σ_0 versus E for $l_c=20$ nm are plotted in Fig. 6, where conductivity rises faster at elevated temperatures.

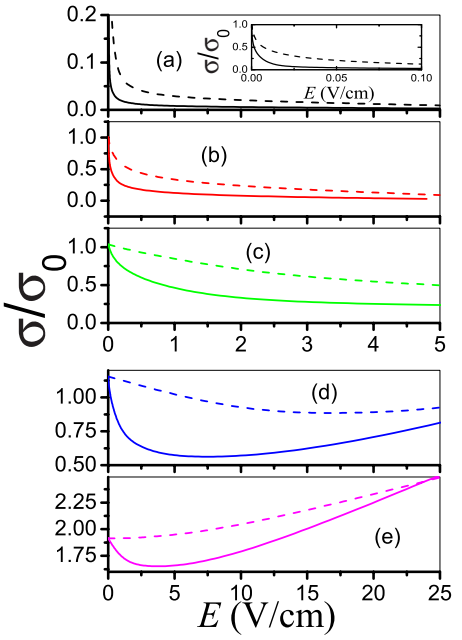

FIG. 5. (Color online) Dimensionless conductivity, σ/σ_0, versus field E for $l_c=10$ nm at different temperatures: (a) $T=4.2$ K, (b) 20 K, (c) 77 K, (d) 150 K, and (e) 300 K. The solid and the dashed curves are calculated from Eqs. (14) and (19), and Eqs. (15)–(19), respectively. Inset in panel (a) shows low-field dependencies.

Figure 7 demonstrates the current-voltage characteristics, i.e., the dependences of the current density $I=\sigma E$ on the electric field E calculated for $l_c=10$ nm at different temperatures. Similar dependences for $l_c=20$ nm are shown in Fig. 8. It is seen that in the range of low temperatures, the current-voltage characteristics can be essentially nonlinear even at relatively small E (corresponding to $I\geq10^{-5}$ A/cm in the low-temperature region). Point out that for larger E and I ($E\geq1$ V/cm at low temperatures and $E\geq10$ V/cm at room temperature), Figs. 7 and 8 present dependences that are close to linear ones. In addition, Figs. 7 and 8 show that in both cases, (i) and (ii), the current-voltage characteristics calculated for given T and l_c are similar. One can also see that current-voltage characteristics can exhibit both sublinear and superlinear behavior in a wide range of the electric field depending on the values of T and l_c. The modification of the current-voltage characteristic shape is attributed to the effects associated with finite values of l_c.

V. CONCLUSIONS

To summarize, we developed the theory of the carries heating in intrinsic graphene in a strong dc electric field for

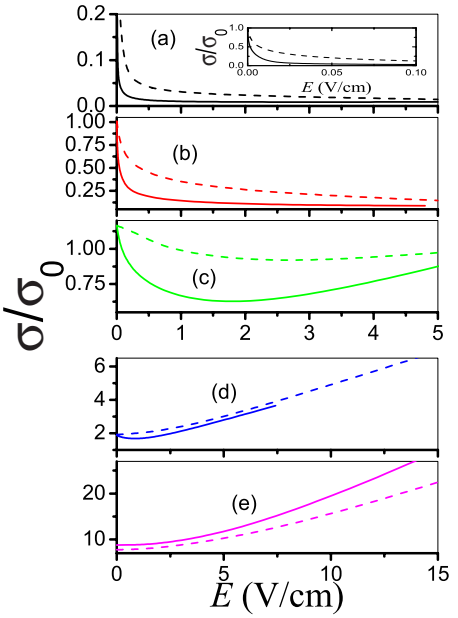

FIG. 6. (Color online) The same as in Fig. 5 for $l_c=20$ nm.

the cases when intercarrier scattering is negligible or dominant. It is found that the deviation from the equilibrium distribution starts from very low electric fields (from 0.3 V/cm at the room temperature and from 10 μV/cm at the liquid-helium temperature) due to ineffective energy relaxation of low energy carriers. Since the energy relaxation sharply intensifies with reinforcing heating and the carrier recombination rate exceeds their thermogeneration, in the short-range

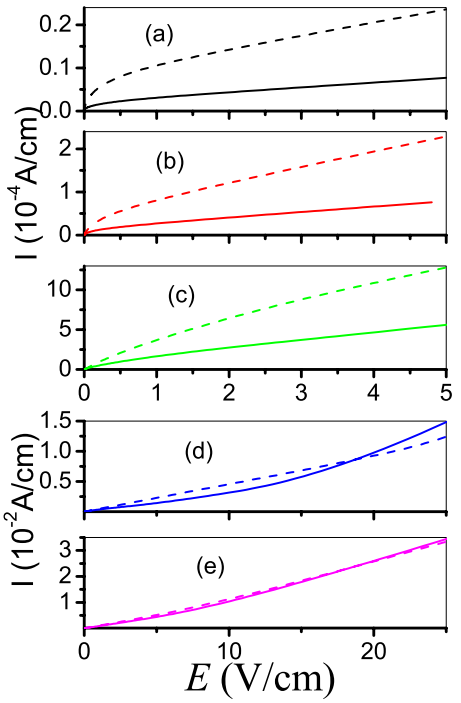

FIG. 7. (Color online) Current-voltage characteristics for $l_c=10$ nm at different temperatures: (a) $T=4.2$ K, (b) 20 K, (c) 77 K, (d) 150 K, and (e) 300 K. The solid and the dashed curves are calculated from Eqs. (14) and (19), and Eqs. (15)–(19), respectively.

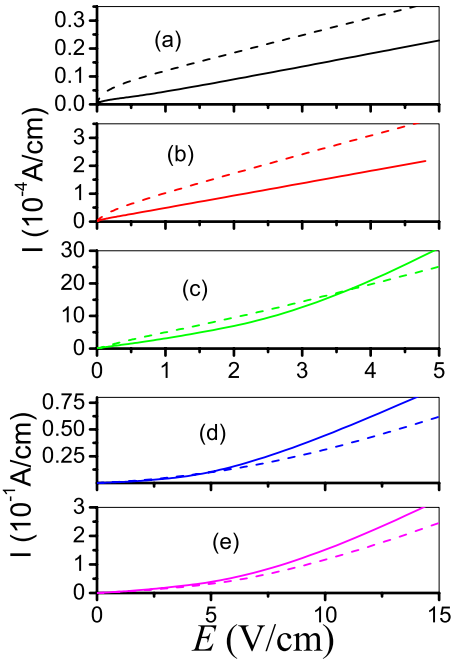

FIG. 8. (Color online) The same as in Fig. 7 for $l_c=20$ nm.

scattering case the current-voltage characteristics can become sublinear. However, in the case of scattering on finite-range disorder, the current-voltage characteristics can demonstrate the superlinear behavior. Therefore, an intrinsic graphene can exhibit a unusual combination of the low threshold of the electric field nonlinearity and appearance of the second ohmic region in strong fields. The dependencies obtained are totally different from the current-voltage characteristics of the bulk gapless semiconductors considered a few decades ago.[18] These differences stem from the qualitative differences of the density of states and the generation-recombination mechanisms. So that in gapless semiconductors a low threshold is not realized while a behavior is similar in the region of a strong field.

Let us discuss the main assumptions made. Here we studied an intrinsic graphene which has at most resistivity so the effect of heating manifests itself the most. Doped materials require a separate investigation, moreover nonlinearity in these materials must be weaker. We have restricted ourselves by the study of limiting cases when the intercarrier Coulomb scattering is either weak or dominating. As shown, the electric field dependences of concentration and the current-voltage characteristics calculated in these two limiting cases are fairly similar, i.e., they exhibit a weak sensitivity to the details of the distribution function. As the main generation-recombination mechanism it is assumed to be associated with the radiative-induced direct interband transitions because the Auger processes are forbidden due to the symmetry of electron-hole states.[14] Possible contribution of other generation-recombination mechanisms (e.g., disorder induced transitions caused by acoustic phonons or carrier-carrier scattering) require an additional investigation. At last, we considered the interaction of carriers with equilibrium thermostats formed by acoustic phonons and radiation (compare with Ref. 19). The problem of heat removal is beyond

of the scope of this paper. We assumed that the heat removal is sufficiently effective.[7] This problem becomes insignificant in the case of sufficiently short electric pulses when the thermostat can be definitely not overheated. The limitations imposed above are because of the lack of data on graphene. Nevertheless, the qualitative pattern of the phenomena studied should not be essentially modified if the mechanisms of relaxation are treated in more details.

The rest of assumptions made above are standard. To describe the momentum relaxation we take into account only the statical disorder scattering using the phenomenological model of Ref. 11 (which is in good agreement with the experimental data; the microscopic mechanisms of scattering are still unclear[20]), whereas a small contribution of acoustic phonons is disregarded. The utilization of the quasielastic approximation for describing of the energy relaxation is justified by condition $v_W \gg s$. The latter ensures the small energy transfer accompanied the scattering process. As the energy of optical phonons is large, their contribution can be neglected even at relatively strong electric fields. An anisotropy of both electron and phonon spectra is also insignificant in the carrier energy ranges under consideration. Since the carrier interaction with thermal radiation can be described by taking into account only of the direct interband transitions (the Drude absorption is small), the approximations used accurately describe the heating mechanism in graphene and lead to correct quantitative description of the electric field dependences of the carrier concentration and the current-voltage characteristics.

In conclusion, the operation of different graphene-based devices, for example, field-effect transistors, as well as the effectiveness of graphene interconnections, can be substantially limited by the carries heating considered above. Apart from this, studies of hot carrier effects can provide valuable information on electron-phonon (hole-phonon) coupling and on the mechanisms of recombination. This makes possible verification of the relaxation mechanisms. Therefore, we believe that the obtained results will stimulate further experimental and theoretical study (as well as numerical modeling) of hot carriers in graphene.

APPENDIX: KINETIC EQUATION

Below we evaluate the system of quasiclassical kinetic equations governing the nonequilibrium carrier distributions in graphene placed in a strong electric field $\mathbf{E}$. Such a consideration is analogous to the approach used for the bulk narrow-gap semiconductors, see Ref. 21 and the recent papers,[10] where a similar approach was developed for the case of graphene. But the case of the bipolar electron-hole plasma was not analyzed in these papers.

We start from the single-particle density matrix which is governed by the quantum kinetic equation[15]

$$\frac{i}{\hbar}[\hat{h}_W - e\mathbf{E}\cdot\mathbf{x}, \hat{\rho}] = \hat{J}_{\text{coll}}. \tag{A1}$$

The collision integral $\hat{J}_{\text{coll}}$ represents the scattering mechanisms (considered in the main text) and $\hat{h}_W$ is the 2×2 Weyl-Wallace Hamiltonian,[22] which describes the states near the band cross point. Here we use the linear dispersion laws $\varepsilon_{lp} = l v_W p$, with l corresponding to the conduction ($l=+1$) or the valence ($l=-1$) bands. The eigenvectors $|l\mathbf{p}\rangle$ are determined from the eigenstate problem as follows:

$$\hat{h}_W|l\mathbf{p}\rangle = \varepsilon_{lp}|l\mathbf{p}\rangle, \quad \hat{h}_W = v_W(\hat{\boldsymbol{\sigma}}\cdot\mathbf{p}),$$

$$|+1\mathbf{p}\rangle = \frac{1}{\sqrt{2}}\begin{vmatrix} 1 \\ e^{i\phi} \end{vmatrix}, \quad |-1\mathbf{p}\rangle = \frac{1}{\sqrt{2}}\begin{vmatrix} -e^{-i\phi} \\ 1 \end{vmatrix}, \tag{A2}$$

where ϕ is the $\mathbf{p}$-plane polar angle. The function describing the distribution over $l\mathbf{p}$ states $F_{l\mathbf{p}} = \langle l\mathbf{p}|\hat{\rho}|l\mathbf{p}\rangle$ and the nondiagonal part of density matrix $\tilde{F}_{\mathbf{p}} = \langle 1\mathbf{p}|\hat{\rho}|-1\mathbf{p}\rangle = \langle -1\mathbf{p}|\hat{\rho}|1\mathbf{p}\rangle^*$ are obtained from the system of kinetic equations

$$e\mathbf{E}\cdot\frac{\partial F_{l\mathbf{p}}}{\partial \mathbf{p}} + l\frac{e}{\hbar}\mathbf{E}\cdot\{\tilde{F}_{\mathbf{p}}\mathbf{X}_{-l,l}(\mathbf{p}) - \mathbf{X}_{l,-l}(\mathbf{p})\tilde{F}^*_{\mathbf{p}}\} = \langle l\mathbf{p}|J_c(\hat{\rho})|l\mathbf{p}\rangle, \tag{A3}$$

$$\frac{i}{\hbar}2v_W p\tilde{F}_{\mathbf{p}} + e\mathbf{E}\cdot\frac{\partial \tilde{F}_{\mathbf{p}}}{\partial \mathbf{p}} + \frac{e}{\hbar}\mathbf{E}\cdot\mathbf{X}_{1,-1}(\mathbf{p})\times(F_{1\mathbf{p}} - F_{-1\mathbf{p}}) + \frac{e}{\hbar}\mathbf{E}\cdot\{\mathbf{X}_{-1,-1}(\mathbf{p}) - \mathbf{X}_{1,1}(\mathbf{p})\}\tilde{F}_{\mathbf{p}} = \langle +1\mathbf{p}|J_c(\hat{\rho})|-1\mathbf{p}\rangle. \tag{A4}$$

Here the interband matrix element of coordinate, $\mathbf{X}_{l,l'}(\mathbf{p}) = \langle l\mathbf{p}|\hat{x}|l'\mathbf{p}\rangle$, is calculated on wave functions of momentum representation (A2) and has the value of the order of $\hbar/\bar{p}$, where $\bar{p}$ is the characteristic momentum of the hot carries.

In order to show the smallness of nondiagonal components of the distribution function, the estimation $\langle l\mathbf{p}|J_c(\hat{\rho})|l\mathbf{p}\rangle \sim F_{l\mathbf{p}}/\tau_m$ is also used, where τ_m is the characteristic time of the momentum relaxation (the smallest characteristic time of the problem). For typical conditions of the applicability of quasiclassical description[13]

$$2v_W\bar{p} \gg \frac{\hbar}{\tau_c}, \quad eE\tau_c \ll \bar{p} \tag{A5}$$

from Eq. (A4) we have estimation $\tilde{F}_{\mathbf{p}}/F_{l\mathbf{p}} \sim \hbar/(2v_W\bar{p}\tau_c)$.

Further, neglecting by small nondiagonal contributions we arrive to the usual system of kinetic equations

$$e\mathbf{E}\cdot\frac{\partial F_{l\mathbf{p}}}{\partial \mathbf{p}} = \sum_j J_j\{F|l\mathbf{p}\}, \tag{A6}$$

which describes the distribution of hot carriers over the bands $l=\pm 1$ and the 2D momentum $\mathbf{p}$. The scattering integrals, $J_j\{F|l\mathbf{p}\}$, are obtained in Refs. 5 and 10. Here l corresponds to conduction ($l=+1$) or valence ($l=-1$) band, $\mathbf{p}$ is the 2D momentum, and $J_j\{F|l\mathbf{p}\}$ is the collision integral for the jth scattering mechanism [$j=D$, LA, R, and C, see discussion after Eq. (1)]. It is convenient to make transition to the electron-hole representation introducing the electron (e)

and hole (h) distribution functions, $f_{e\mathbf{p}}$ and $f_{e\mathbf{p}}$, according to the replacements[23]

$$F_{+1,\mathbf{p}} \to f_{e\mathbf{p}}, \quad 1 - F_{-1,\mathbf{p}t} \to f_{h\mathbf{p}} \tag{A7}$$

and to rewrite the collision integrals in Eq. (A6) through $f_{e,h\mathbf{p}}$.

Finally, using substitution (A7) and the velocity operator $\hat{\mathbf{v}} = i[\hat{h}_W, \mathbf{x}]/\hbar = v_W \hat{\boldsymbol{\sigma}}$, we obtain the velocity of $l\mathbf{p}$ state: $\langle l\mathbf{p}|\hat{\mathbf{v}}|l\mathbf{p}\rangle = l v_W \mathbf{p}/p \equiv \mathbf{v}_{l\mathbf{p}}$. Taking into account fourfold degeneracy of states in graphene due to spin and valley degrees of freedom, one obtains the current density

$$\mathbf{I} = \frac{4e}{L^2}\sum_{l\mathbf{p}} \mathbf{v}_{l\mathbf{p}} F_{l\mathbf{p}} = \frac{4ev_W}{L^2}\sum_{\mathbf{p}} \frac{\mathbf{p}}{p}(f_{e\mathbf{p}} + f_{h\mathbf{p}}). \tag{A8}$$

In addition, in the intrinsic material the electron density is equal to the hole one (the neutrality condition) as follows:

$$\frac{4}{L^2}\sum_{\mathbf{p}} (f_{e\mathbf{p}} - f_{h\mathbf{p}}) = 0. \tag{A9}$$

Thus, the symmetric scattering for the c and the v bands Eqs. (A6), (A8), and (A9) preserve their form when $f_{e\mathbf{p}}$ is replaced by $f_{h\mathbf{p}}$. As a result, the electron and hole distributions in the intrinsic material are identical, $f_{e\mathbf{p}} = f_{h\mathbf{p}} \equiv f_{\mathbf{p}}$ so that the kinetic equation and the current density take the forms of Eqs. (1) and (3), respectively.

*ftvasko@yahoo.com

[1] A. H. Castro Neto, F. Guinea, N. M. R. Peres, K. S. Novoselov, and A. K. Geim, Rev. Mod. Phys. **81**, 109 (2009).

[2] P. Avouris, Z. Chen, and V. Perebeinos, Nat. Nanotechnol. **2**, 605 (2007); P. Avouris and J. Chen, Mater. Today **9**, 46 (2006).

[3] D. Sun, Z.-K. Wu, C. Divin, X. Li, C. Berger, W. A. de Heer, P. N. First, and T. B. Norris, Phys. Rev. Lett. **101**, 157402 (2008).

[4] S. Butscher, F. Milde, M. Hirtschulz, E. Malic, and A. Knorr, Appl. Phys. Lett. **91**, 203103 (2007).

[5] F. T. Vasko and V. Ryzhii, Phys. Rev. B **77**, 195433 (2008).

[6] M. C. Lemme, T. J. Echtermeyer, M. Baus, and H. Kurz, IEEE Electron Device Lett. **28**, 282 (2007); Y. Q. Wu, P. D. Ye, M. A. Capano, Y. Xuan, Y. Sui, M. Qi, J. A. Cooper, T. Shen, D. Pandey, G. Prakash, and R. Reifenberger, Appl. Phys. Lett. **92**, 092102 (2008); X. Wang, Y. Ouyang, X. Li, H. Wang, J. Guo, and H. Dai, Phys. Rev. Lett. **100**, 206803 (2008).

[7] J. Moser, A. Barreiro, and A. Bachtold, Appl. Phys. Lett. **91**, 163513 (2007).

[8] E. H. Hwang, Ben Yu-Kuang Hu, and S. Das Sarma, Phys. Rev. B **76**, 115434 (2007); W.-K. Tse and S. Das Sarma, arXiv:0812.1008 (unpublished).

[9] A. Akturk and N. Goldsman, J. Appl. Phys. **103**, 053702 (2008).

[10] M. Auslender and M. I. Katsnelson, Phys. Rev. B **76**, 235425 (2007); S. V. Syzranov, M. V. Fistul, and K. B. Efetov, *ibid.* **78**, 045407 (2008).

[11] F. T. Vasko and V. Ryzhii, Phys. Rev. B **76**, 233404 (2007).

[12] T. Stauber, N. M. R. Peres, and F. Guinea, Phys. Rev. B **76**, 205423 (2007); N. M. R. Peres, J. M. B. Lopes dos Santos, and T. Stauber, *ibid.* **76**, 073412 (2007); F. Guinea, J. Low Temp. Phys. **153**, 359 (2008).

[13] L. Fritz, J. Schmalian, M. Müller, and S. Sachdev, Phys. Rev. B **78**, 085416 (2008); M. Müller, L. Fritz, and S. Sachdev, *ibid.* **78**, 115406 (2008).

[14] M. S. Foster and I. L. Aleiner, Phys. Rev. B **79**, 085415 (2009).

[15] F. T. Vasko and O. E. Raichev, *Quantum Kinetic Theory and Applications* (Springer, New York, 2005).

[16] The relation $A_p + p(dA_p/dp)/2 = [d(p^2 A_p)/dp]/2p$ is used in Eq. (8).

[17] D. Potter, *Computational Physics* (Wiley, London, 1973).

[18] S. D. Beneslavskii and A. V. Dmitriev, Solid State Commun. **32**, 1175 (1979); B. A. Akimov, A. V. Dmitriev, D. R. Khokhlov, and L. I. Ryabova, Phys. Status Solidi A **137**, 9 (1993); S. D. Beneslavskii and O. Ziep, Phys. Status Solidi B **88**, 221 (2006).

[19] P. N. Romanets, F. T. Vasko, and M. V. Strikha, Phys. Rev. B **79**, 033406 (2009).

[20] T. M. Mohiuddin, L. A. Ponomarenko, R. Yang, S. M. Morozov, A. A. Zhukov, F. Schedin, E. W. Hill, K. S. Novoselov, M. I. Katsnelson, and A. K. Geim, arXiv:0809.1162 (unpubished); S. Adam, P. W. Brouwer, and S. Das Sarma, arXiv:0811.0609 (unpublished).

[21] I. M. Dykman, V. M. Rosenbaum, and F. T. Vasko, Phys. Status Solidi B **88**, 385 (1978).

[22] E. M. Lifshitz, L. P. Pitaevskii, and V. B. Berestetskii, *Quantum Electrodynamics* (Butterworth-Heinemann, Oxford, 1982); P. R. Wallace, Phys. Rev. **71**, 622 (1947).

[23] A. I. Anselm, *Introduction to Semiconductor Theory* (Prentice-Hall, Englewood Cliffs, NJ, 1981); since there is no magnetic field under consideration, we do not reverse a momentum direction and the sign of charge ($e < 0$).